Supplementary Information for Monitoring Spatially Heterogeneous Subsidence of Transportation Infrastructure in Beijing Using Sentinel-1 InSAR Time Series

Weizhen Lin [1, 2], Yidi Wang[1, 2] ,Changyang Hu[1, 2] and Zhang Yunjun [1, 2,*]

1 National Key Laboratory of Microwave Imaging, Aerospace Information Research Institute, Chinese Academy of Sciences, Beijing 100094, China

2 School of Electronic, Electrical and Communication Engineering, University of Chinese Academy of Sciences,Beijing 100049, China

*** Correspondence: yunjunz@aircas.ac.cn**

Figure S1. Perpendicular baseline history for Sentinel-1 ascending track A142 and descending track D47

Figure S2. Interferogram network for Sentinel-1 ascending track A142 and descending track D47.

Figure S3. Coherence history for Sentinel-1 ascending track A142 and descending track D47

Figure S4. Temporal coherence map for Sentinel-1 ascending track A142 / descending track D47.

Figure S5. Triplet-closure error map for Sentinel-1 ascending track A142 and descending track D47.

Figure S6. Cumulative subsidence and subsidence gradient along the Ring Expressway.

Figure S7. Cumulative subsidence and subsidence gradient along the Expressway.

Figure S8. Cumulative subsidence and subsidence gradient along the airport runway .

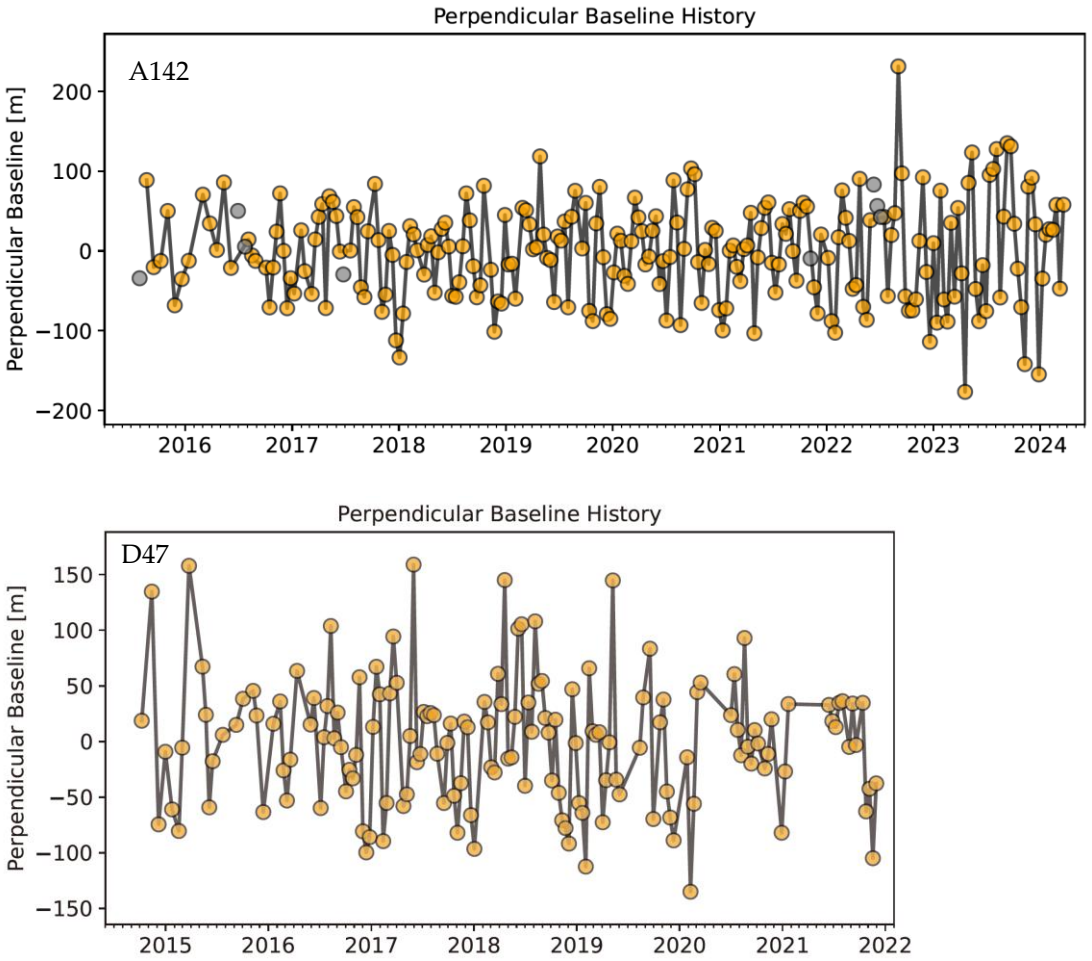

Figure S1. Perpendicular baseline history for Sentinel-1 ascending track A142 and descending track D47. The Sentinel-1 ascending acquisitions show generally stable perpendicular baselines from 2016 to 2024, mostly within ±150 m. Occasional larger values occur, but the overall distribution remains consistent and suitable for interferogram generation. The descending acquisitions display a comparable baseline pattern between 2015 and 2022, with most baselines also within ±150 m. The stable geometry supports reliable interferometric processing for the descending dataset.

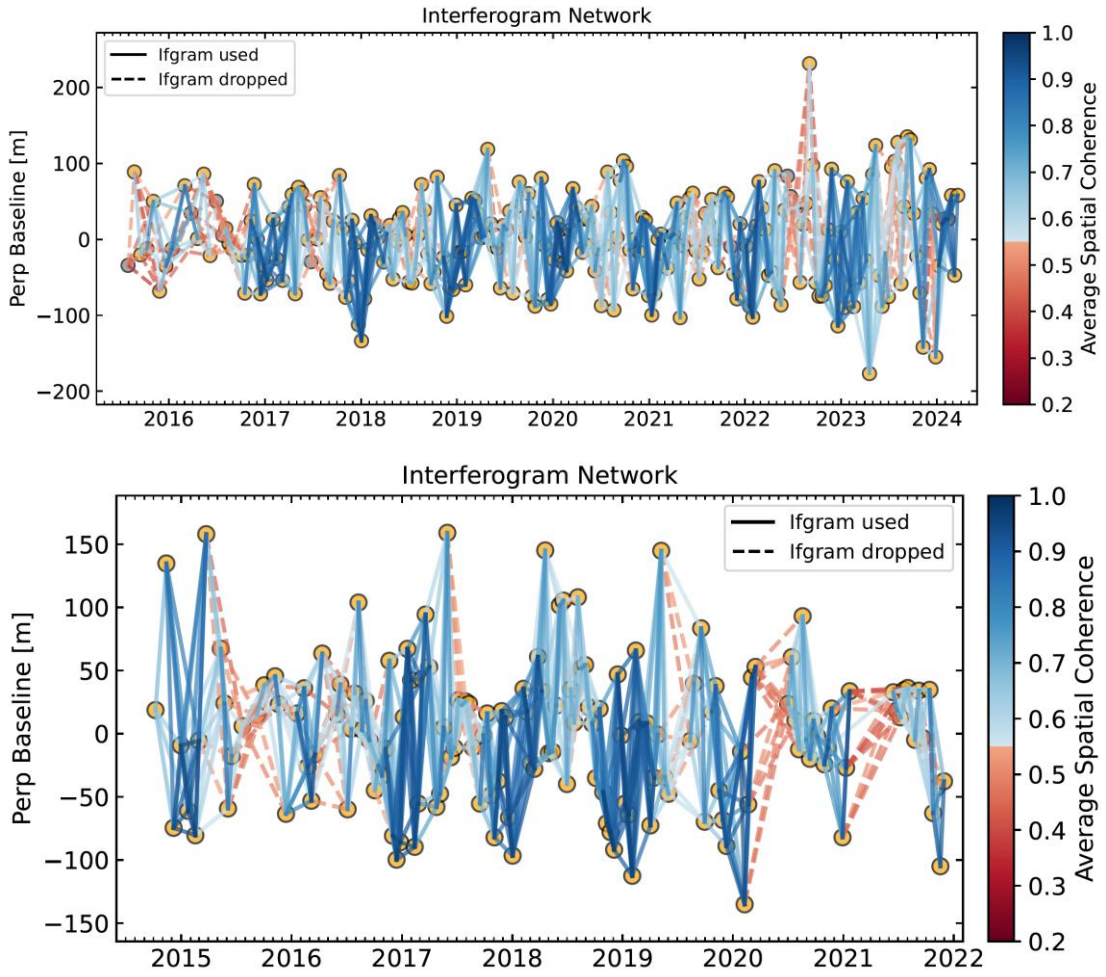

Figure S2. Interferogram network for Sentinel-1 ascending track A142 and descending track D47. Interferogram network for the Sentinel-1 ascending track A142 (top) and descending track D47 (bottom). Solid blue lines represent interferograms retained for SBAS processing, whereas dashed red lines indicate those discarded based on the coherence threshold. Line color corresponds to the average spatial coherence, illustrating the temporal and geometric distribution of interferogram quality across the dataset.

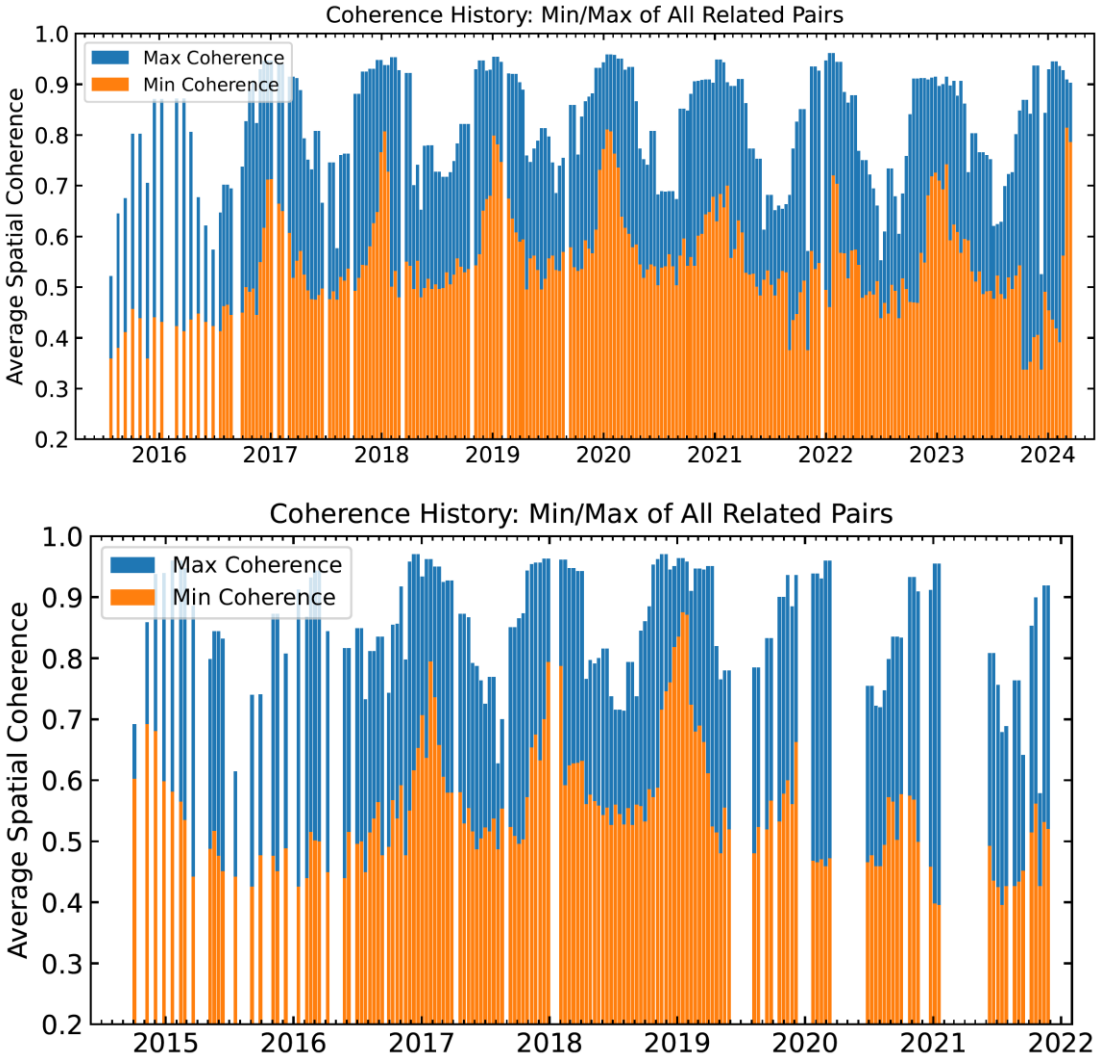

Figure S3. Coherence history for the Sentinel-1 ascending track A142 (top) and descending track D47 (bottom). The plots show the minimum and maximum average spatial coherence of all interferogram pairs over time. Both tracks maintain generally stable and sufficiently high coherence, indicating consistently good interferometric data quality and supporting the reliability of the phase unwrapping and subsequent time-series deformation results.

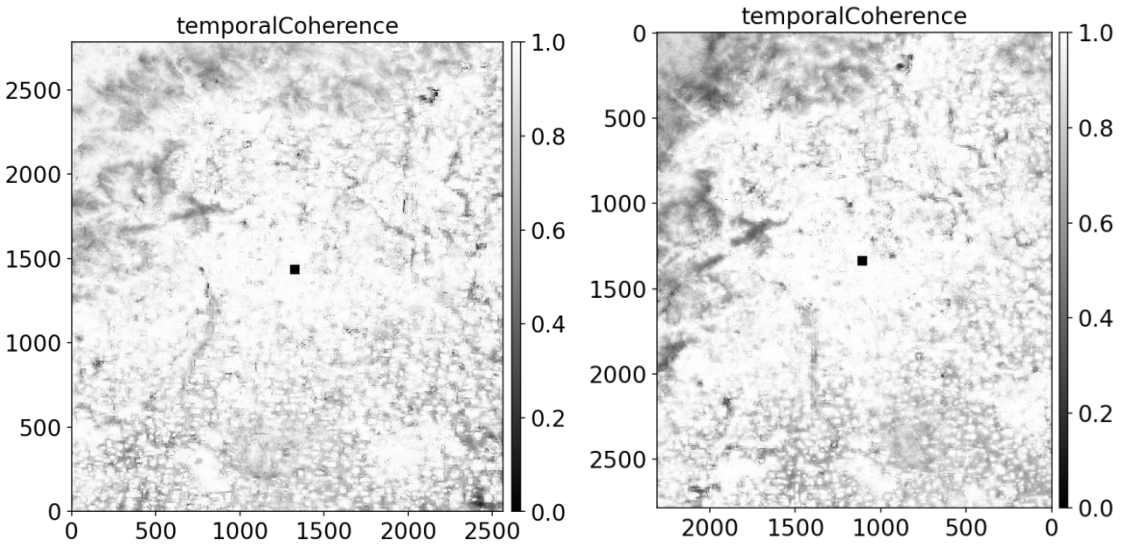

Figure S4. Temporal coherence maps for the Sentinel-1 ascending track A142 (left) and descending track D47 (right). The maps show the long-term mean coherence derived from all interferogram pairs, illustrating the spatial variability of phase stability across the study area. High-coherence regions indicate stable surfaces suitable for reliable time-series inversion, whereas low-coherence areas correspond to decorrelation caused by vegetation, land cover changes, or water bodies.

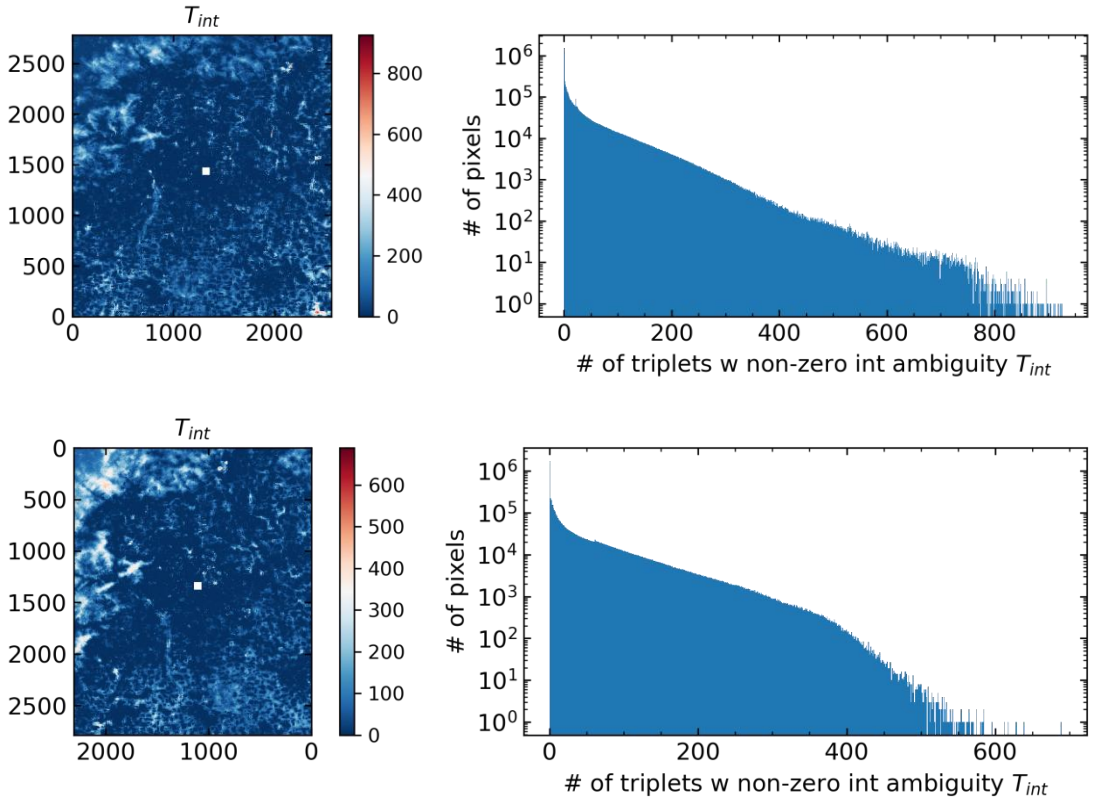

Figure S5. Triplet - closure validation for the Sentinel-1 ascending track A142 (top) and descending track D47 (bottom). The maps show the number of interferogram triplets exhibiting non-zero integer ambiguities, while the accompanying histograms present their frequency distribution across all coherent pixels. For both tracks, the vast majority of pixels exhibit zero or very few closure inconsistencies, indicating that the interferometric phase is internally self-consistent. The low triplet-closure counts confirm that the unwrapped phases are reliable and that no significant unwrapping errors propagate through the interferogram network.

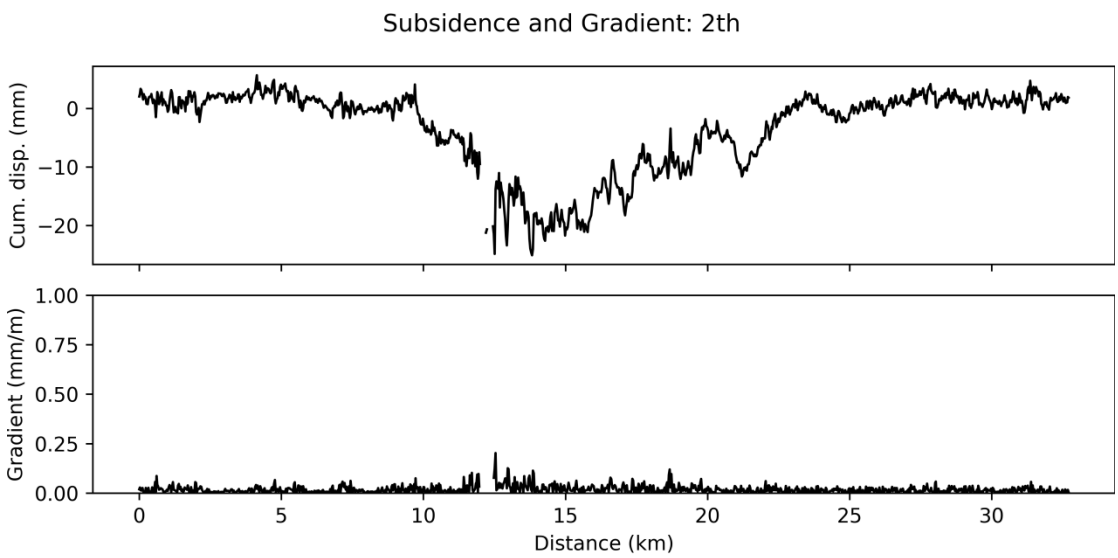
Subsidence and Gradient: 2th
Cum. disp. (mm)
0
−10
−20
Gradient (mm/m)
1.00
0.75
0.50
0.25
0.00
0
5
10
15
20
25
30
Distance (km)

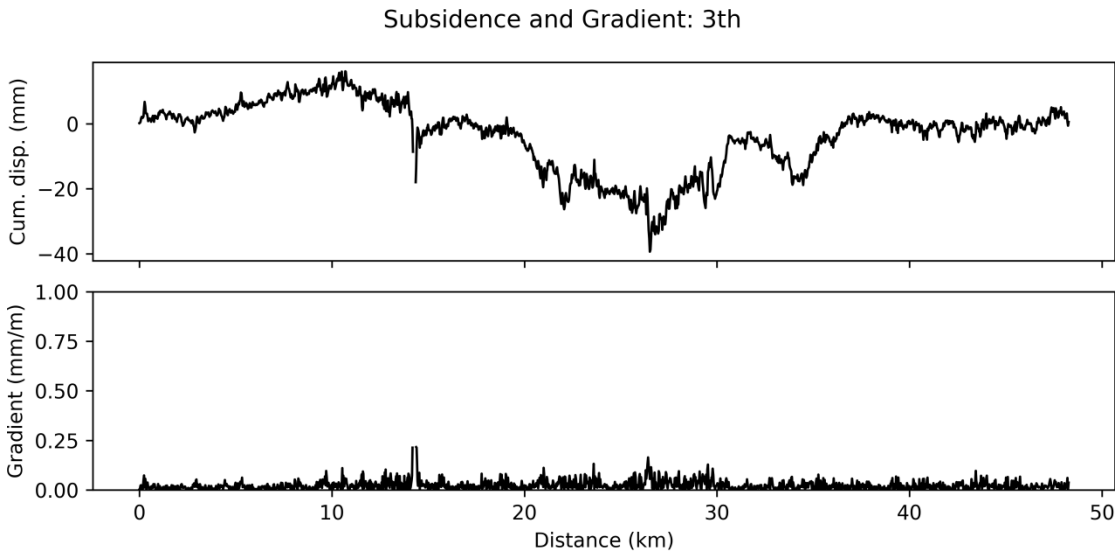
Subsidence and Gradient: 3th
Cum. disp. (mm)
0
−20
−40
Gradient (mm/m)
1.00
0.75
0.50
0.25
0.00
0
10
20
30
40
50
Distance (km)

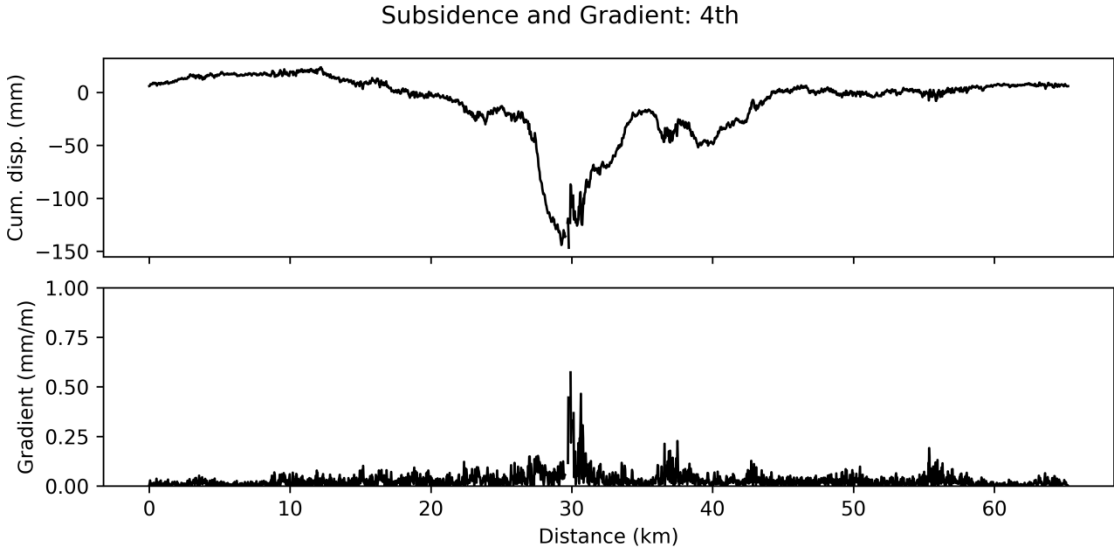
Subsidence and Gradient: 4th
Cum. disp. (mm)
0
−50
−100
−150
Gradient (mm/m)
1.00
0.75
0.50
0.25
0.00
0
10
20
30
40
50
60
Distance (km)

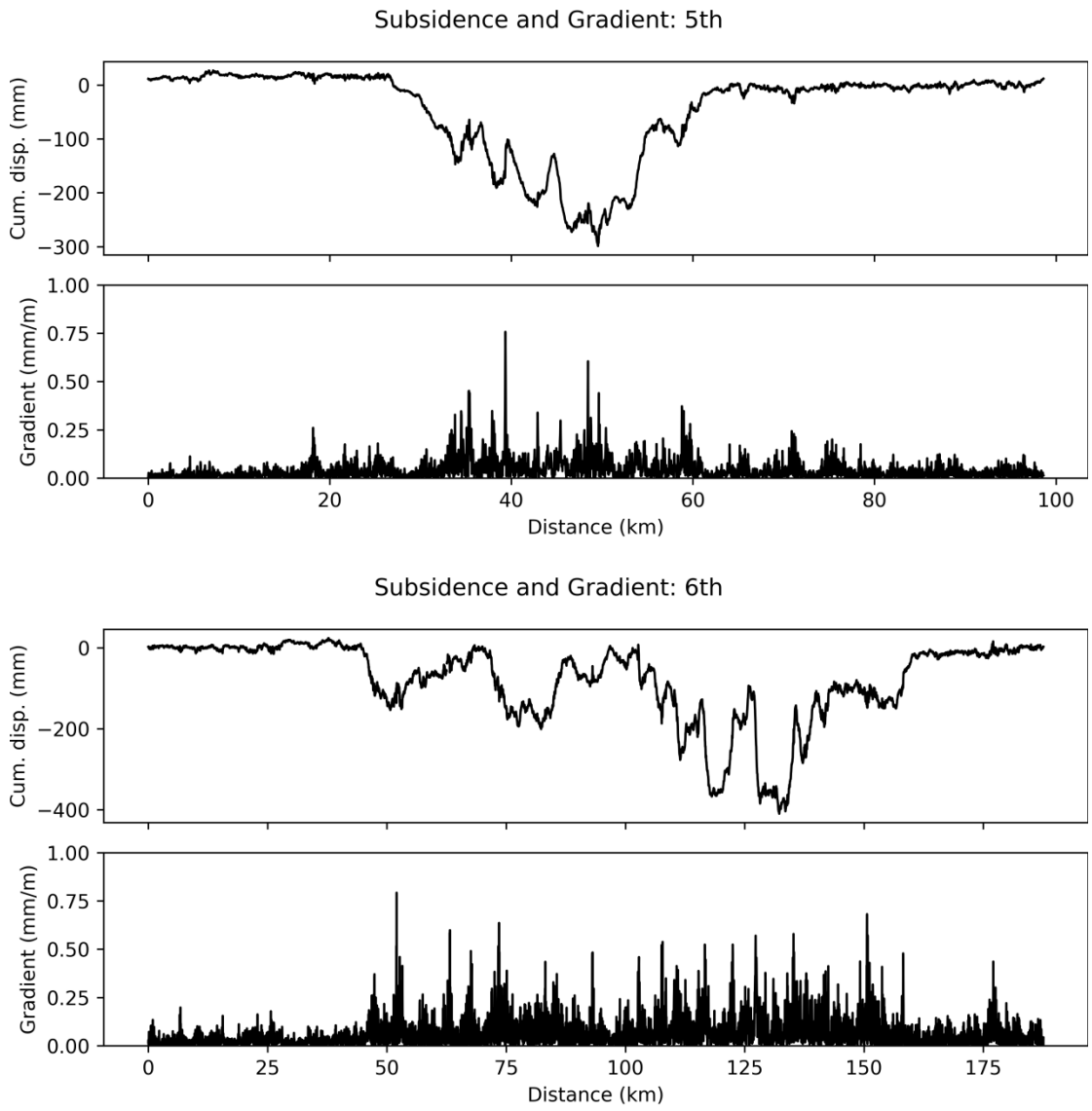

Figure S6. Cumulative subsidence and subsidence gradient along the Ring Expressway.The cumulative displacement curves reveal the long-term settlement pattern, while the gradient profiles highlight localized deformation zones where displacement changes rapidly. The 2nd Ring Road shows a cumulative displacement range from −26.91 to 5.18 mm, with a maximum gradient of 0.24 mm/m; the 3rd Ring Road ranges from −38.94 to 16.31 mm, with a maximum gradient of 0.23 mm/m; the 4th Ring Road ranges from −146.68 to 23.70 mm, with a maximum gradient of 0.57 mm/m; the 5th Ring Road ranges from −300.05 to 27.16 mm, with a maximum gradient of 0.71 mm/m; and the 6th Ring Road ranges from −406.94 to 24.17 mm, with a maximum gradient of 0.72 mm/m.

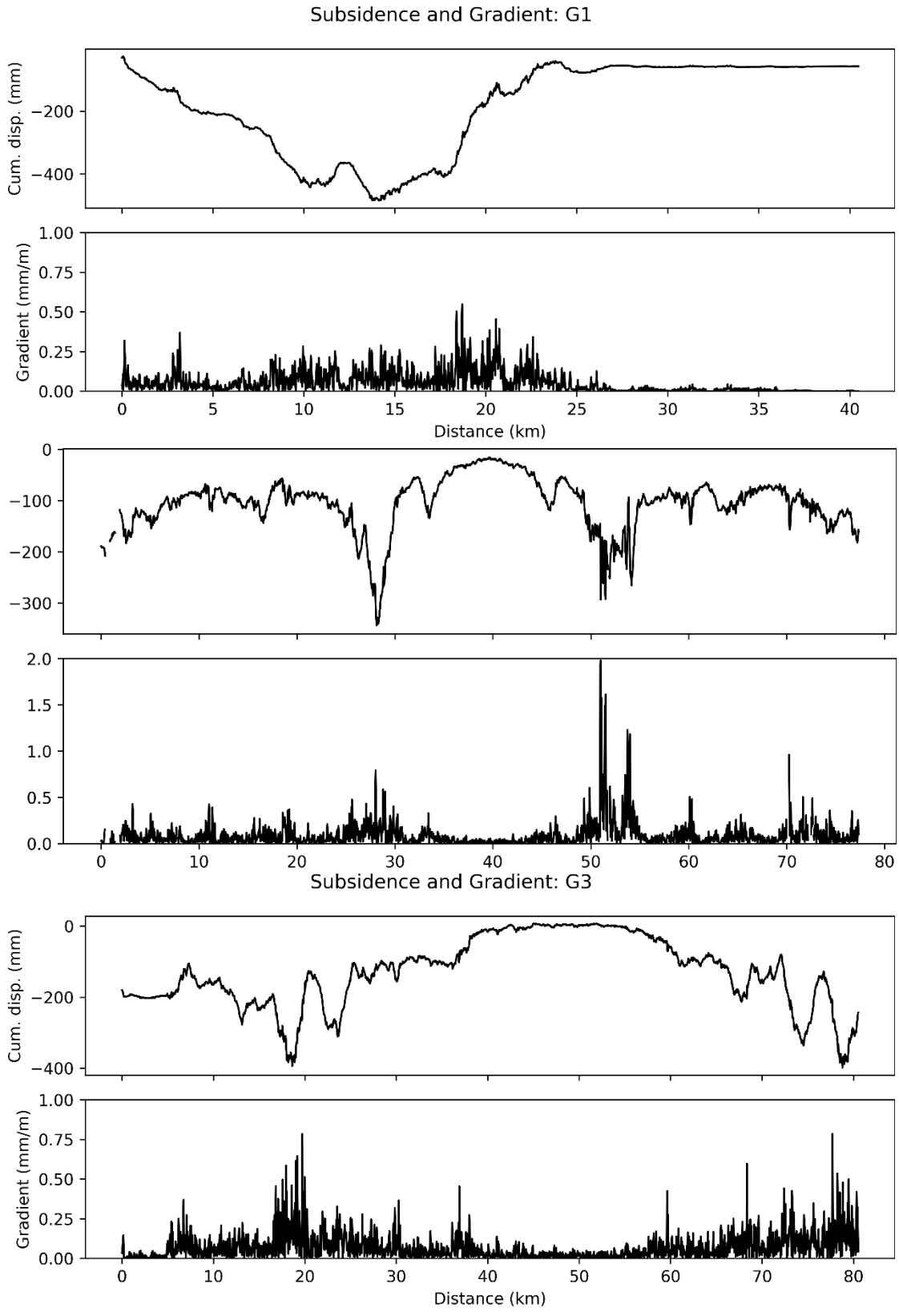
Subsidence and Gradient: G1
Cum. disp. (mm)
−200
−400
Gradient (mm/m)
1.00
0.75
0.50
0.25
0.00
0
5
10
15
20
25
30
35
40
Distance (km)
0
−100
−200
−300
2.0
1.5
1.0
0.5
0.0
0
10
20
30
40
50
60
70
80
Subsidence and Gradient: G3
Cum. disp. (mm)
0
−200
−400
Gradient (mm/m)
1.00
0.75
0.50
0.25
0.00
0
10
20
30
40
50
60
70
80
Distance (km)

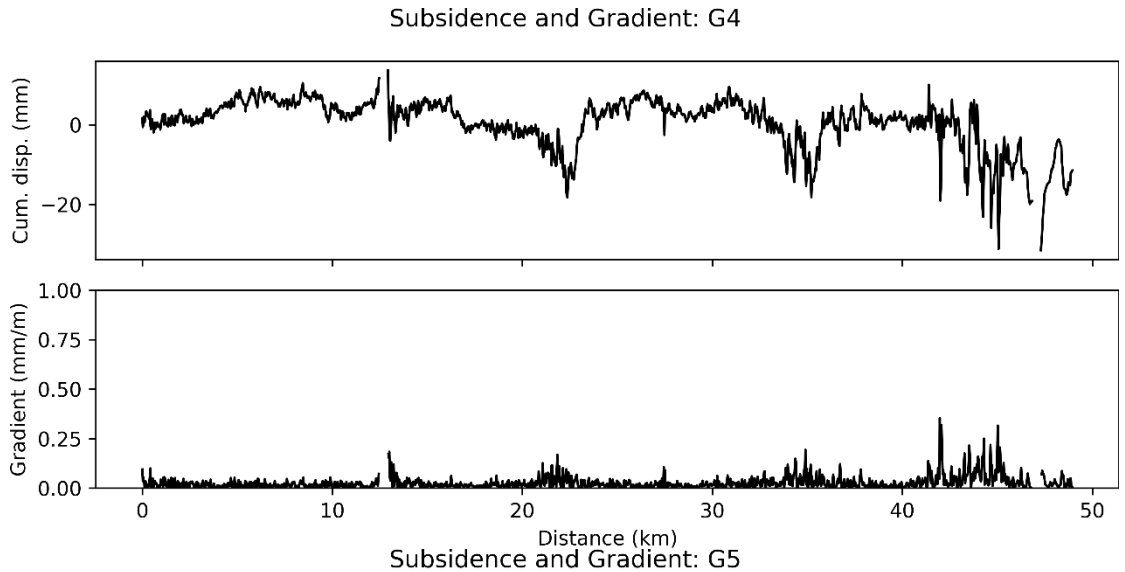
Subsidence and Gradient: G4
Cum. disp. (mm)
0
−20
Gradient (mm/m)
1.00
0.75
0.50
0.25
0.00
0
10
20
30
40
50
Distance (km)

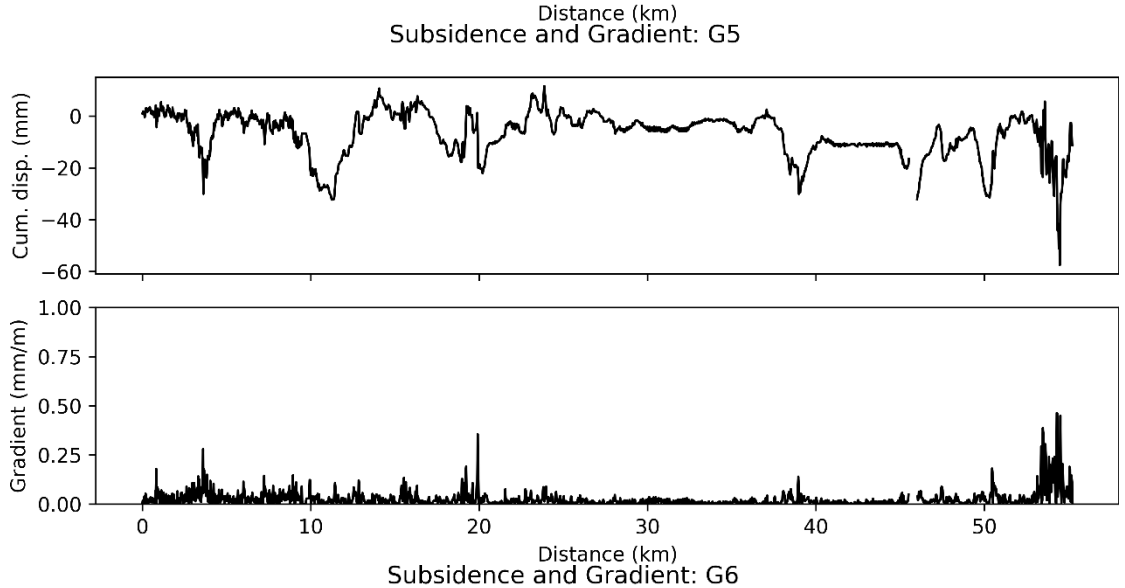
Subsidence and Gradient: G5
Cum. disp. (mm)
0
−20
−40
−60
Gradient (mm/m)
1.00
0.75
0.50
0.25
0.00
0
10
20
30
40
50
Distance (km)

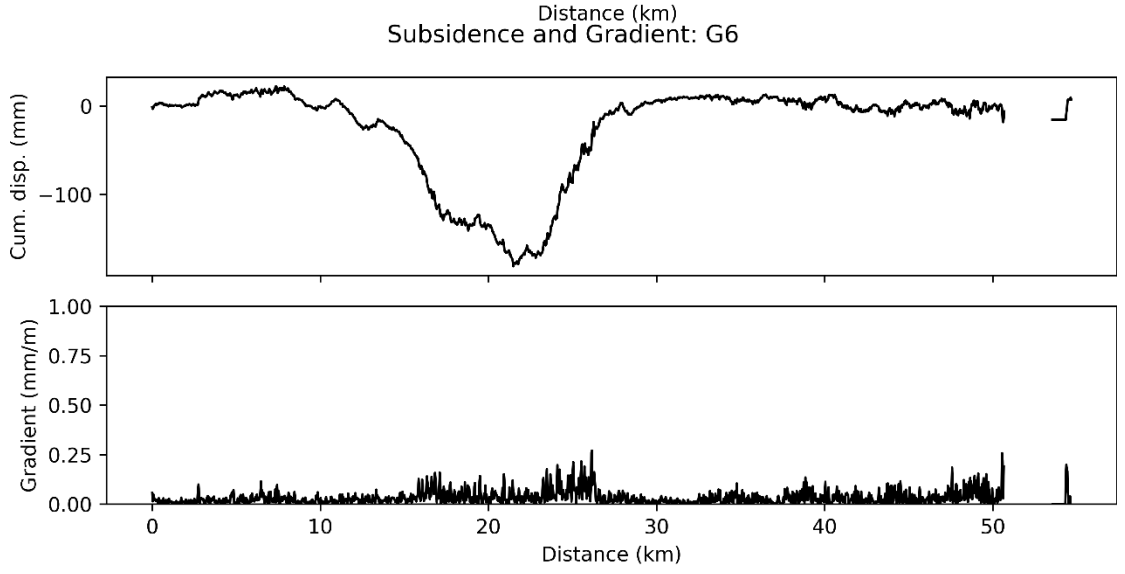
Subsidence and Gradient: G6
Cum. disp. (mm)
0
−100
Gradient (mm/m)
1.00
0.75
0.50
0.25
0.00
0
10
20
30
40
50
Distance (km)

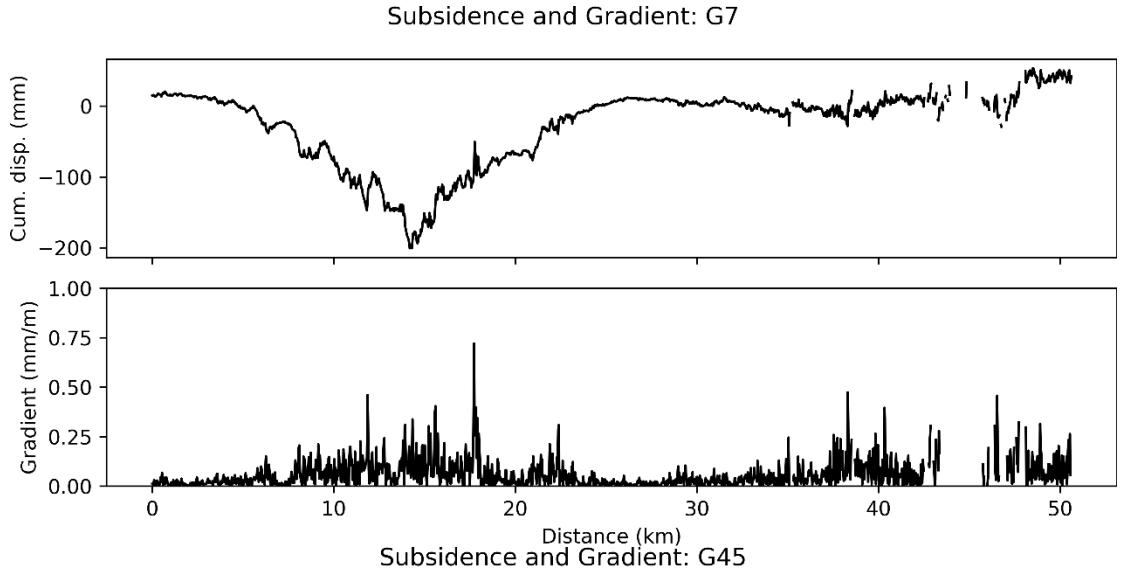
Subsidence and Gradient: G7
Cum. disp. (mm)
0
−100
−200
Gradient (mm/m)
1.00
0.75
0.50
0.25
0.00
0
10
20
30
40
50
Distance (km)

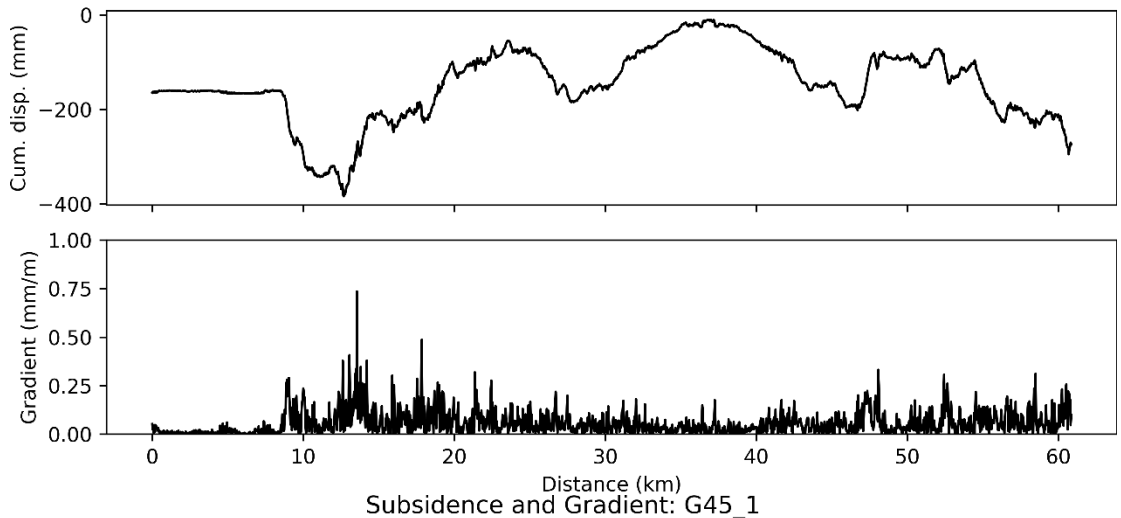
Subsidence and Gradient: G45
Cum. disp. (mm)
0
−200
−400
Gradient (mm/m)
1.00
0.75
0.50
0.25
0.00
0
10
20
30
40
50
60
Distance (km)

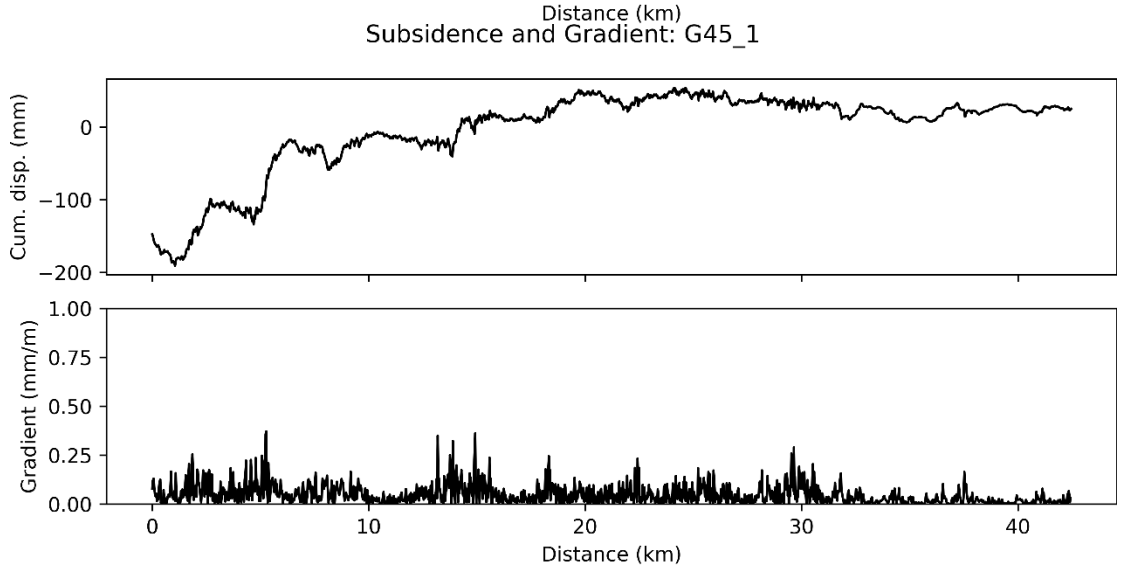
Subsidence and Gradient: G45_1
Cum. disp. (mm)
0
−100
−200
Gradient (mm/m)
1.00
0.75
0.50
0.25
0.00
0
10
20
30
40
Distance (km)

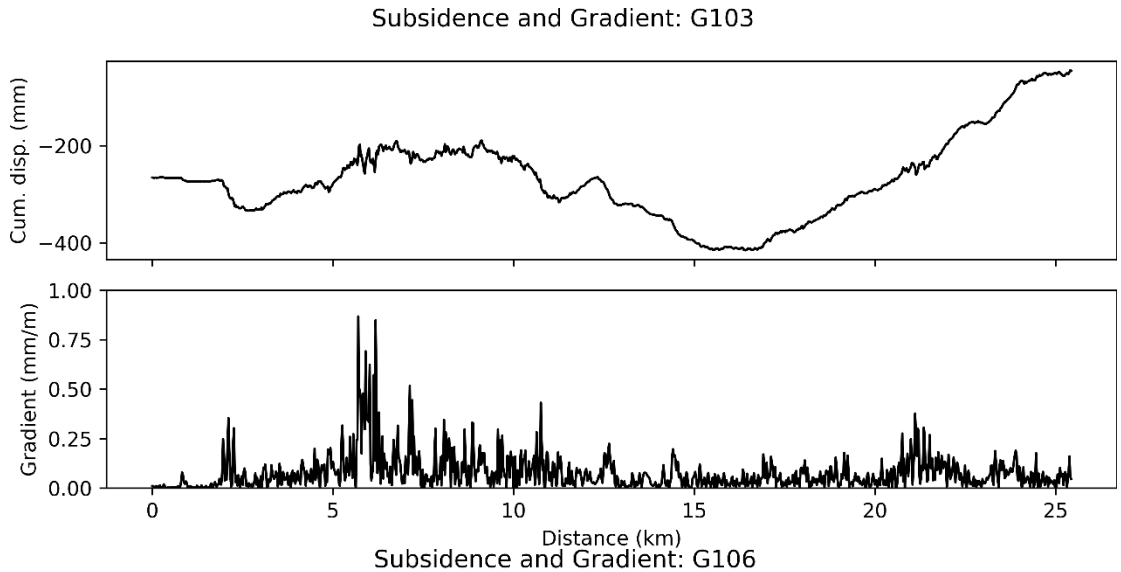
Subsidence and Gradient: G103
Cum. disp. (mm)
−200
−400
Gradient (mm/m)
1.00
0.75
0.50
0.25
0.00
0
5
10
15
20
25
Distance (km)

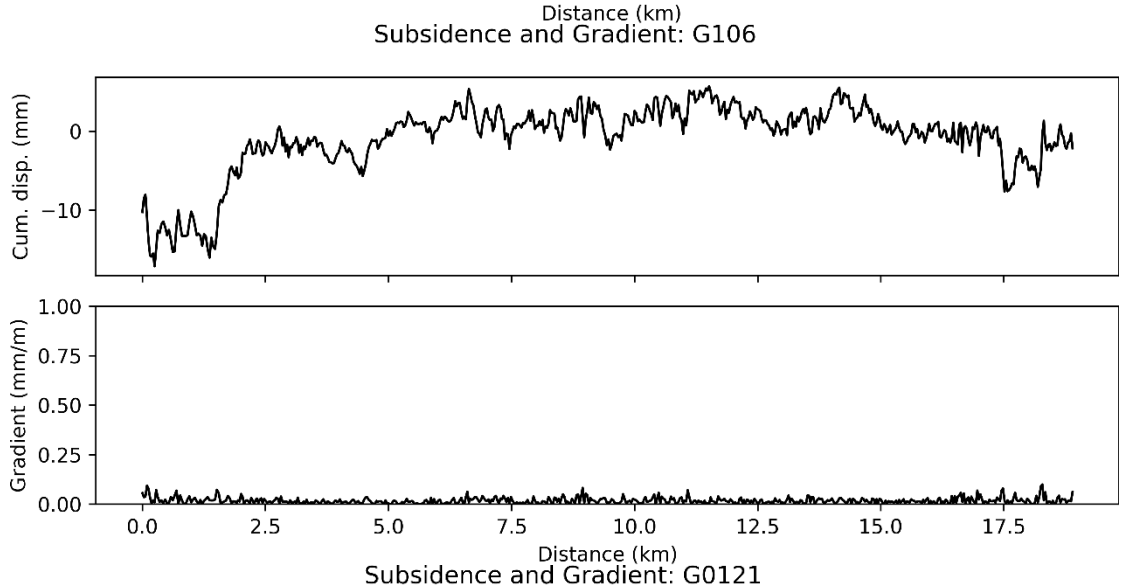
Subsidence and Gradient: G106
Cum. disp. (mm)
0
−10
Gradient (mm/m)
1.00
0.75
0.50
0.25
0.00
0.0
2.5
5.0
7.5
10.0
12.5
15.0
17.5
Distance (km)

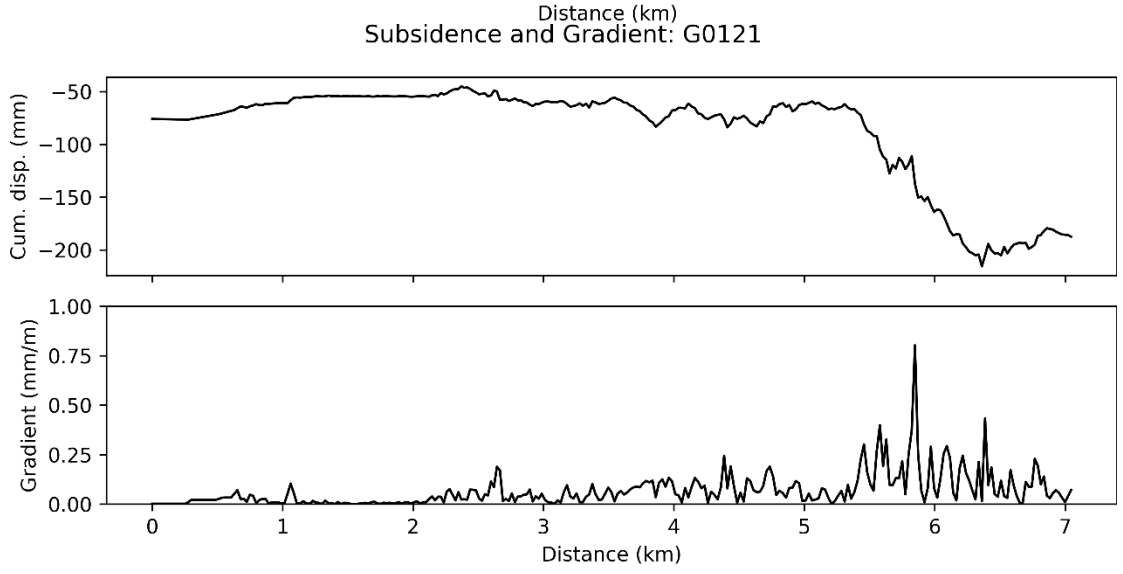
Subsidence and Gradient: G0121
Cum. disp. (mm)
−50
−100
−150
−200
Gradient (mm/m)
1.00
0.75
0.50
0.25
0.00
0
1
2
3
4
5
6
7
Distance (km)

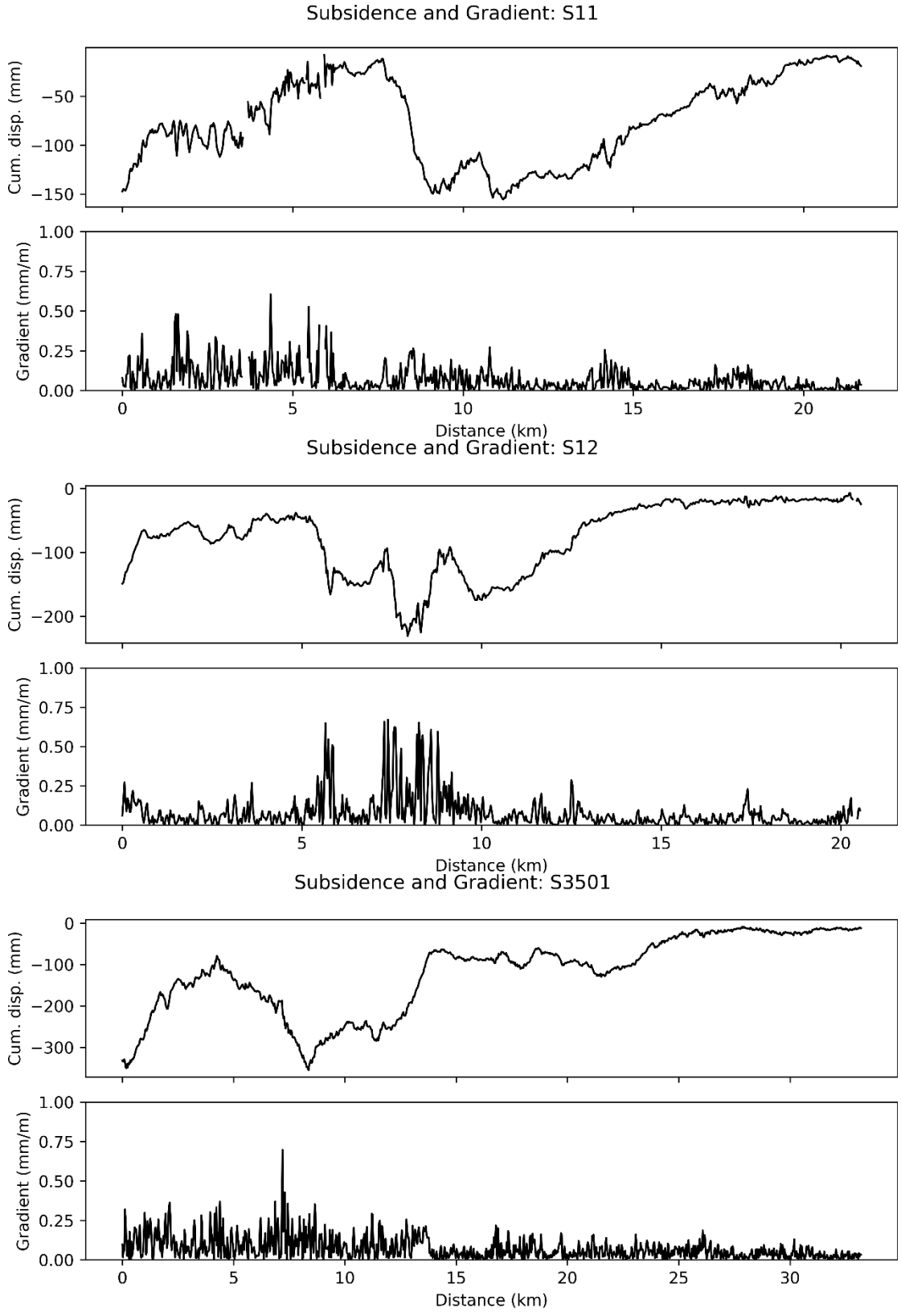

Figure S7. Cumulative subsidence and subsidence gradient along the Expressway.The cumulative displacement curves illustrate the overall settlement pattern, and the gradient profiles identify locations with rapid deformation changes. The G1 segment shows a cumulative displacement range from −484.18 to −26.04 mm, with a maximum gradient of 0.55 mm/m; G2 ranges from −343.82 to −15.59 mm, with a maximum gradient of 1.98 mm/m; G3

ranges from −399.12 to 7.50 mm, with a maximum gradient of 0.78 mm/m; G4 ranges from −31.48 to 13.68 mm, with a maximum gradient of 0.35 mm/m; G5 ranges from −57.50 to 11.50 mm, with a maximum gradient of 0.46 mm/m; G6 ranges from −180.93 to 22.45 mm, with a maximum gradient of 0.27 mm/m; G7 ranges from −200.77 to 53.46 mm, with a maximum gradient of 0.72 mm/m; G45 ranges from −383.68 to −9.98 mm, with a maximum gradient of 0.74 mm/m; G45-1 ranges from −190.95 to 54.02 mm, with a maximum gradient of 0.37 mm/m; G103 ranges from −415.58 to −44.67 mm, with a maximum gradient of 0.87 mm/m; G106 ranges from −17.13 to 5.68 mm, with a maximum gradient of 0.10 mm/m; G0121 ranges from −215.54 to −44.93 mm, with a maximum gradient of 0.80 mm/m; S11 ranges from −155.48 to −7.58 mm, with a maximum gradient of 0.61 mm/m; S12 ranges from −230.68 to −7.11 mm, with a maximum gradient of 0.67 mm/m; and S3501 ranges from −355.27 to −8.47 mm, with a maximum gradient of 0.70 mm/m.

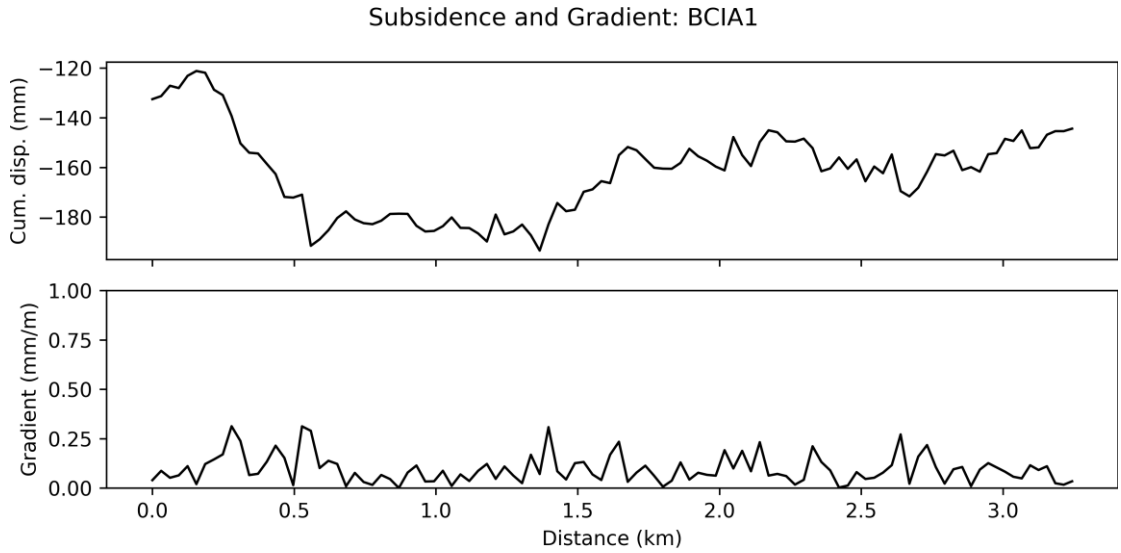
Subsidence and Gradient: BCIA1
Cum. disp. (mm)
−120
−140
−160
−180
Gradient (mm/m)
1.00
0.75
0.50
0.25
0.00
0.0
0.5
1.0
1.5
2.0
2.5
3.0
Distance (km)

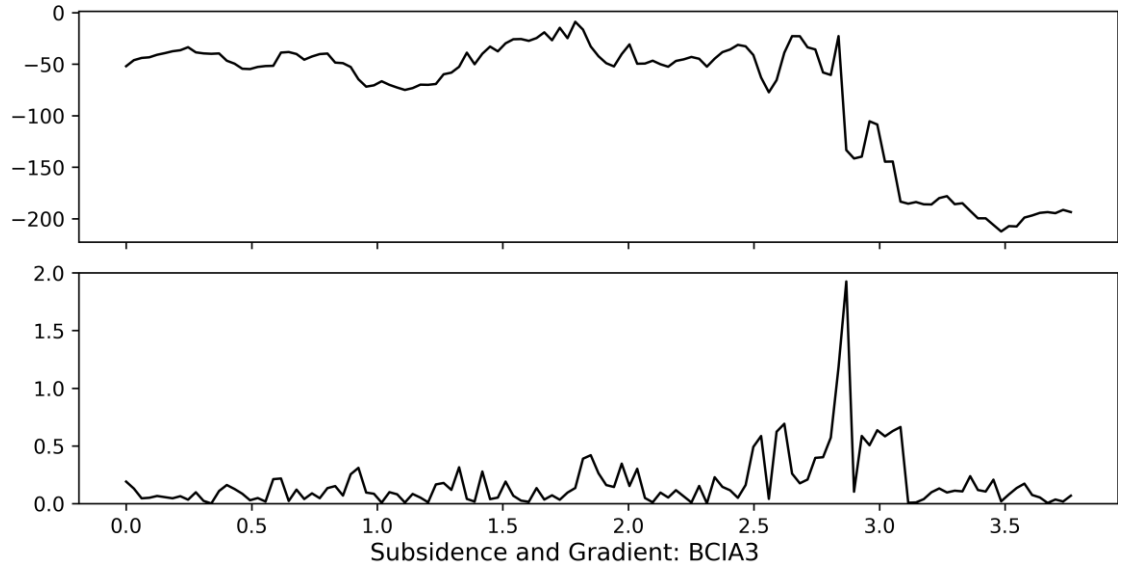
0
−50
−100
−150
−200
2.0
1.5
1.0
0.5
0.0
0.0
0.5
1.0
1.5
2.0
2.5
3.0
3.5

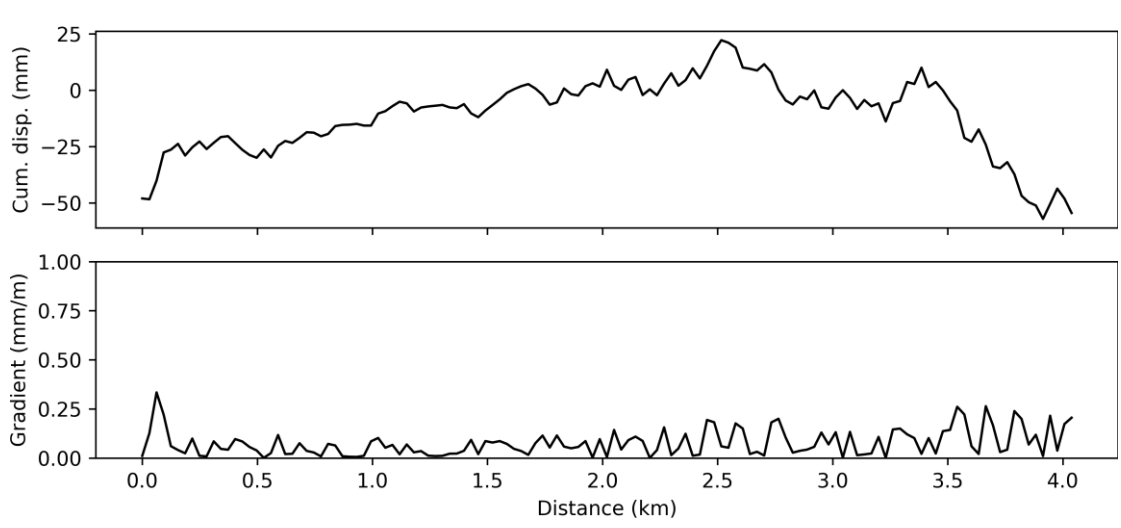
Subsidence and Gradient: BCIA3
Cum. disp. (mm)
25
0
−25
−50
Gradient (mm/m)
1.00
0.75
0.50
0.25
0.00
0.0
0.5
1.0
1.5
2.0
2.5
3.0
3.5
4.0
Distance (km)

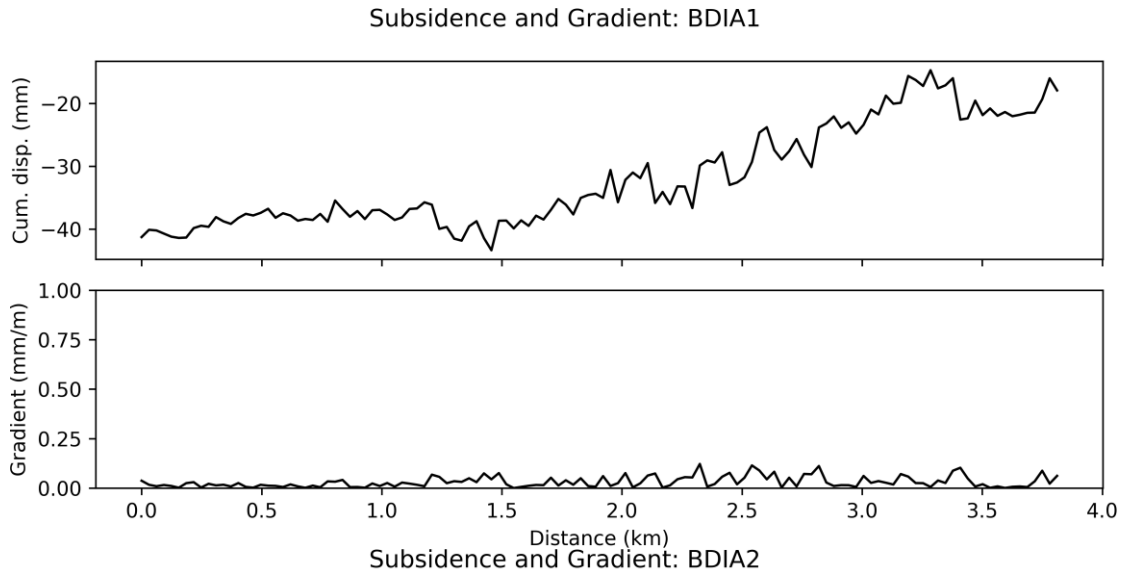
Subsidence and Gradient: BDIA1
Cum. disp. (mm)
−20
−30
−40
Gradient (mm/m)
1.00
0.75
0.50
0.25
0.00
0.0
0.5
1.0
1.5
2.0
2.5
3.0
3.5
4.0
Distance (km)

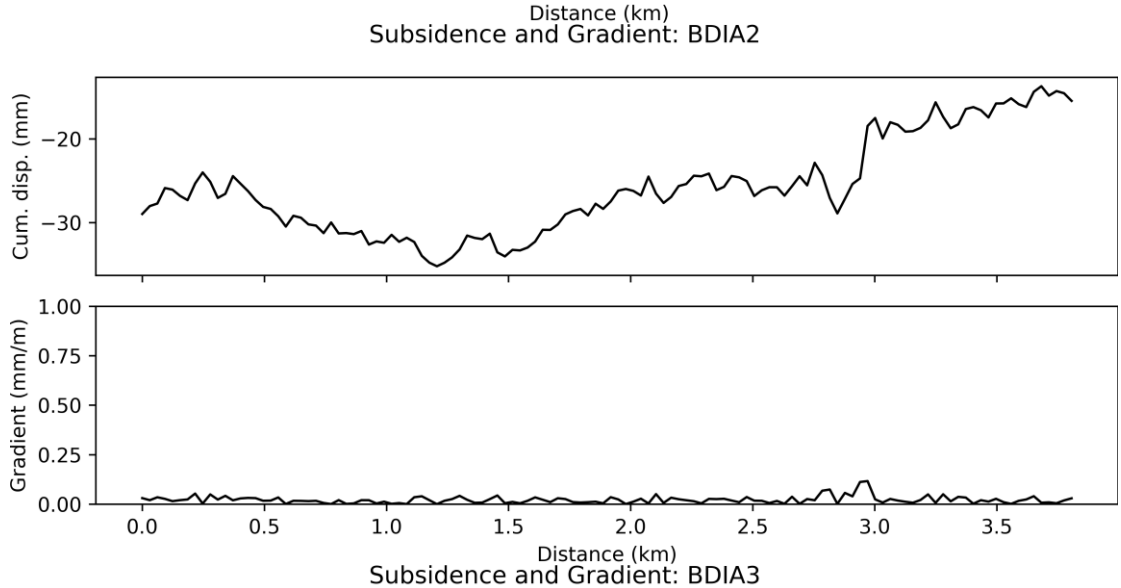
Subsidence and Gradient: BDIA2
Cum. disp. (mm)
−20
−30
Gradient (mm/m)
1.00
0.75
0.50
0.25
0.00
0.0
0.5
1.0
1.5
2.0
2.5
3.0
3.5
Distance (km)

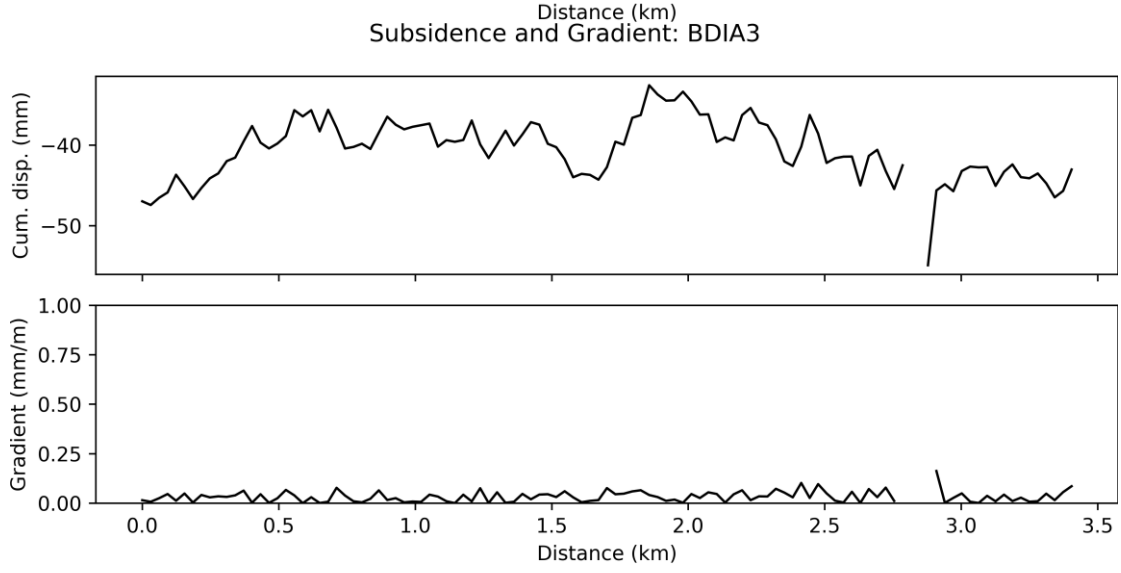
Subsidence and Gradient: BDIA3
Cum. disp. (mm)
−40
−50
Gradient (mm/m)
1.00
0.75
0.50
0.25
0.00
0.0
0.5
1.0
1.5
2.0
2.5
3.0
3.5
Distance (km)

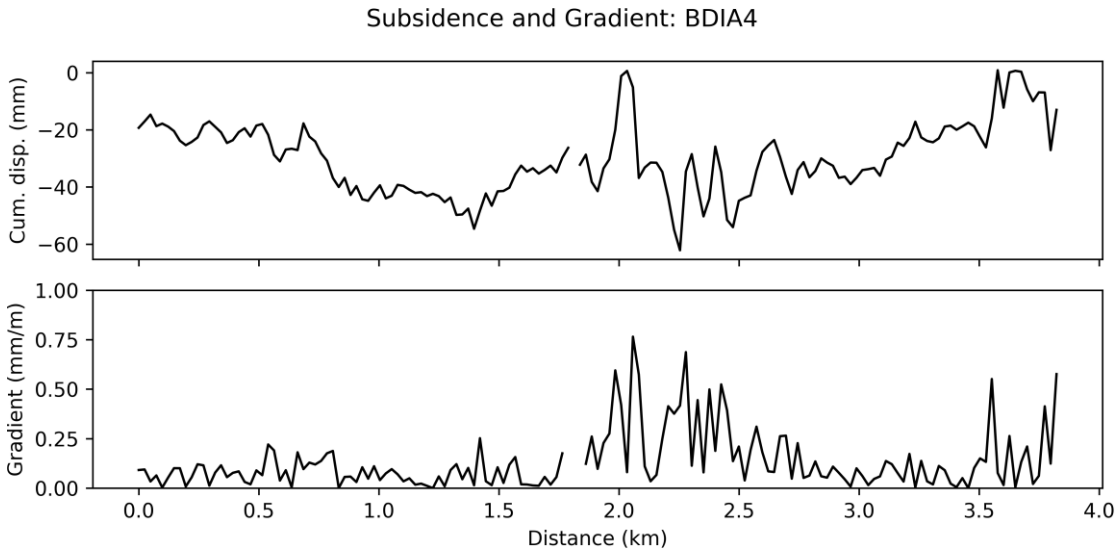

Figure S8. Cumulative subsidence and subsidence gradient along the airport runway .The cumulative displacement curves present the overall settlement distribution, and the gradient profiles indicate locations with rapid deformation transitions. The BCIA1 runway segment shows a cumulative displacement range from −193.49 to −121.15 mm, with a maximum gradient of 0.31 mm/m; BCIA2 ranges from −212.39 to −8.91 mm, with a maximum gradient of 1.93 mm/m; BCIA3 ranges from −57.08 to 22.16 mm, with a maximum gradient of 0.33 mm/m. The BDIA1 segment ranges from −43.38 to −14.69 mm, with a maximum gradient of 0.12 mm/m; BDIA2 ranges from −35.23 to −13.71 mm, with a maximum gradient of 0.12 mm/m; BDIA3 ranges from −54.93 to −32.58 mm, with a maximum gradient of 0.16 mm/m; and BDIA4 ranges from −62.15 to 0.89 mm, with a maximum gradient of 0.77 mm/m.